A Space-Time Model for Frequency Nonselective Rayleigh Fading Channels with Applications to Space-Time Modems

Tai-Ann Chen, *Member, IEEE*, Michael P. Fitz, *Member, IEEE*, Wen-Yi Kuo, *Senior Member, IEEE*, Michael D. Zoltowski, *Fellow, IEEE*, and Jimm H. Grimm

***Abstract*—This paper extends the traditional Clarke/Jakes model for a frequency flat fading process in a land mobile radio system to facilitate the examination of coherent space-time demodulation systems. The work develops a space-time correlation function using a ring of scatterers model around the mobile unit. The resulting correlation function permits the investigation of a variety of issues concerning base station configurations in space-time systems. The interrelationship of the fading process between the space and the time domain is explored. A detailed example regarding the effects of antenna separation in a receiver diversity system is considered. A set of design rules for interleaving depth and antenna separation in a space-time modem is presented and quantified.**

***Index Terms*—Antenna separation, diversity, interleaving depth, Rayleigh fading channel, space-time channel correlation.**

I. Introduction

DIVERSITY techniques provide significant performance improvements for fading channels. Typical diversity techniques include time diversity, frequency diversity, and spatial diversity. Designs with combinations of these schemes have also been proposed to improve the communication quality. For techniques involving multiple antennas, it is usually assumed that the respective signal paths between spatially separated antennas and the mobile receiver are reasonably uncorrelated. Although this can be achieved by making the relative antenna separation (AS) large, it may not always be feasible due to the space limitation. One example of combining temporal and spatial diversity is the recent proposals for space-time coded modulations (STCM) [1], [2]. Although channel correlations can be compensated by the code design of STCM when the fading process is fixed, typical assumptions in work on STCM still assume the spatial channels are uncorrelated when considering time-varying fading. This condition is often hard to satisfy especially at low carrier frequencies. To explore the effects of a space-time communication link geometry on the performance, we propose a space-time model for narrowband radio channels. This model is then used to parameterize performance as a function of AS and the interleaving depth (ID).

The proposed model is a space-time generalization of the work by Clarke/Jakes [3], [4] and produces a statistical model for examining the effect of AS and ID on the performance of a space-time modem. A more detailed and realistic model of propagation has been developed by Aulin [5] and Parsons and Turkmani [6], [7] that facilitates the examination of vertical antenna displacement. Our interest was characterizing the effect of the horizontal separation, so these models were not adopted for the generalization. The extension of the approach to these models, however, would be straightforward. Most existing models [3], [4], [6], [7] were focused on either the temporal correlation at a fixed location or the instantaneous spatial correlation. The new statistical model explores the interrelationship between these correlations, and allows us to draw some conclusions as to the effects of ID and AS on space-time modem performance.

The paper is organized as follows. Section II describes the model, the cross-correlation function, and the cross-spectrum function. Section III investigates various AS design issues. A few properties regarding the space-time diversity and the performance characterization metrics are examined in Section IV. Section V dictates the space-time modem AS and ID design, and Section VI contains a few concluding remarks. The detailed derivation of the space-time cross-correlation and cross-spectrum functions is in Appendix I, while the analytical pairwise symbol error probability (SEP) over correlated channels with perfect channel state information (CSI) is derived in Appendix II.

II. A Channel Model

The base station (BS) antennas in land mobile radio systems are usually well above city buildings with no major scatterers nearby, while the mobile station (MS) is frequently immersed in a complex scattering environment. A typical scenario for the wireless transmission between one MS antenna and two BS antennas can be modeled as Fig. 1, where a scatterer ring is placed around the MS to model the multipath reflectors [3]. These scatterers are assumed to be uniformly distributed on the ring, and each scatterer has an independent, uniformly distributed initial phase over $[-\pi, \pi]$. This model is not intended to accurately

Manuscript received September 28, 1998; revised April 24, 1999 and November 10, 1999.

T.-A. Chen is with the Wireless Systems Core Technology Department, Lucent Technologies, Whippany, NJ 07981 USA (e-mail: tac@lucent.com).

M. P. Fitz is with the Department of Electrical Engineering, The Ohio State University, Columbus, OH 43210-1272 USA (e-mail: Fitz.7@osu.edu).

W.-Y. Kuo is with WISCOM Technologies, Clark, NJ 07066 USA (e-mail: wkuo@ieee.org).

M. D. Zoltowski is with the School of Electrical and Computer Engineering, Purdue University, West Lafayette, IN 47907 USA (e-mail: mikedz@ecn.purdue.edu).

J. H. Grimm is with Grayson Wireless, Herndon, VA 20170 USA (e-mail: jimm@ieee.org).

Publisher Item Identifier S 0733-8716(00)05410-X.

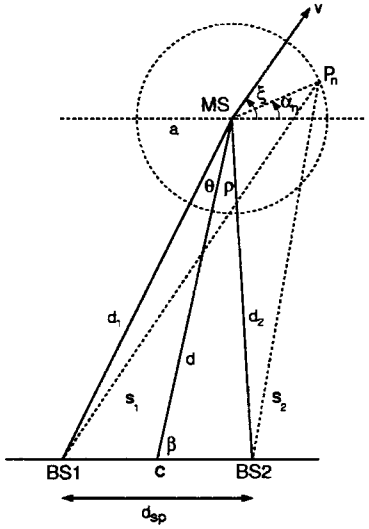

Fig. 1. The transmission model between a mobile and the base station.

describe individual channel realizations but to represent an "average" channel for the purpose of macroscopic system design tradeoffs. In addition, the applicability of the model to a fixed wireless system where the Doppler spread is mainly due to the motion of scatterers is not clear. Note that the antennas in the model are all assumed to be omnidirectional, but directional antennas can be easily accommodated.

The flat fading channel distortions from each of the two BS antennas are

$$c_1(t) = \sqrt{\frac{\sigma^2}{N}} \sum_{n=1}^{N} \exp\{j[2\pi f_D t \cos(\xi - \alpha_n) + \phi_n]\} \tag{1}$$

$$c_2(t) = \sqrt{\frac{\sigma^2}{N}} \sum_{n=1}^{N} \exp\{j[2\pi f_D t \cos(\xi - \alpha_n) + \phi_n - \Delta\phi_n]\} \tag{2}$$

where, referring to Fig. 1, N is the number of reflectors, σ^2 is the variance of the channel, f_D is Doppler spread caused by the vehicle movement, α_n is the angle of the nth reflector on the scatterer ring, i.e., $\alpha_n = 2\pi n/N$, ξ is the angle of vehicle motion, ϕ_n is the initial phase of the nth scatterer received at the first antenna, and $\Delta\phi_n$ is the phase difference caused by the path length difference from the nth scatterer to the two BS antennas. The angles described here are all with respect to the positive horizontal line. Note that the $\Delta\phi_n$ is deterministic and can be evaluated by $\Delta\phi_n = 2\pi(s_1 - s_2)/\lambda$ where λ is the carrier wavelength. The phase ϕ_n will be modeled as uniformly distributed on $[-\pi, \pi]$. This channel model is a generalization of the ring of scatterers model given in [3] in the sense that we consider coherent detection as opposed to noncoherent detection.

The generalized space-time cross-correlation function and the cross-spectrum function can be derived from the proposed model. We detail the derivations in Appendix I. The space (d_{sp})-time (τ) cross-correlation can be represented as

$$\begin{aligned}\rho &= R_{c_1c_2}(\tau, d_{sp}) \\ &= \sigma^2 \exp\left[j\frac{2\pi}{\lambda}(d_1 - d_2)\right] \\ &\quad \times J_0\left[2\pi\sqrt{\left(f_D\tau\cos\xi + \frac{z_c}{\lambda}\right)^2 + \left(f_D\tau\sin\xi - \frac{z_s}{\lambda}\right)^2}\right]\end{aligned} \tag{3}$$

and the space-time cross-spectrum can be written as

$$\begin{aligned}&S_{c_1c_2}(f, d_{sp}) \\ &\quad = \sigma^2 \exp\left[j\frac{2\pi}{\lambda}(d_1 - d_2)\right] \\ &\qquad \times \frac{\cos\left(\frac{2\pi}{\lambda f_D}(z_c\sin\xi + z_s\cos\xi)\sqrt{1 - \left(\frac{f}{f_D}\right)^2}\right)}{\pi f_D\sqrt{1 - \left(\frac{f}{f_D}\right)^2}}\end{aligned} \tag{4}$$

where $J_0[.]$ is the Bessel function of the first kind of order zero

$$z_c = \frac{2a}{d_1 + d_2}[d_{sp} - (d_1 - d_2)\cos\theta\cos\beta] \tag{5}$$

$$z_s = \frac{2a}{d_1 + d_2}(d_1 - d_2)\cos\theta\sin\beta. \tag{6}$$

The fundamental parameters of this model are summarized as follows (refer to Fig. 1 for other parameters):

- a scatterer ring radius;
- d mobile distance to the center of the antenna pair;
- β mobile position angle with respect to the end-fire of the antennas;
- ξ mobile moving direction with respect to the end-fire of the antennas;
- f_D the Doppler spread.

All the other parameters in the model are functions of these parameters, e.g., $d_1 = g_1(d, d_{sp}, \beta)$.

The space-time correlation and the space-time spectrum are not real-valued functions. The space-time model induces a deterministic Doppler frequency independent phase shift (unimportant for the performance evaluation), and a Doppler frequency and other geometric parameters dependent amplitude modulation compared to the classic U-shaped spectrum of [3] and [4]. Unless specified differently, the term correlation as used in this paper refers to its magnitude for the purpose of comparison. Also, $\sigma^2 = 1$ is assumed in this paper.

When comparing the spatial and temporal correlations to the existing model [3], it is noted that as $d_{sp} \to 0$, the cross-correlation function and the cross-spectrum reduce to the single-channel autocorrelation function and spectrum derived in [3] and [4] $\sigma^2 J_0(2\pi f_D\tau)$ and $\sigma^2(\pi f_D\sqrt{1 - (f/f_D)^2})^{-1}$, respectively. As for $\tau \to 0$, it can be shown that although the cross-correlation function takes a different representation from the instantaneous spatial correlation derived in [3], the maximal magnitude difference between them is of order of 10^{-4} over the parameter range of interest.

A plot of $|R_{c_1c_2}(\tau, d_{sp})|$ is shown in Fig. 2 for the parameters $d = 1000\lambda$, $a = 25\lambda$, $\beta = \pi/6$, $\xi = 5\pi/12$, and $f_DT = 0.02$, where T is the symbol period. Note the temporal variations are solely a function of f_D and the spatial variations are a function of the model geometry and λ. A plot of $|S_{c_1c_2}(f, d_{sp} = 30.6\lambda)|$ for the same geometry as Fig. 2 is shown in Fig. 3.

III. Antenna Separation and Receiver Diversity

The major goal of this work is for the space-time modem design to quantify the selection of AS and ID, and calculate the respective system performance. Our approach to joint AS and

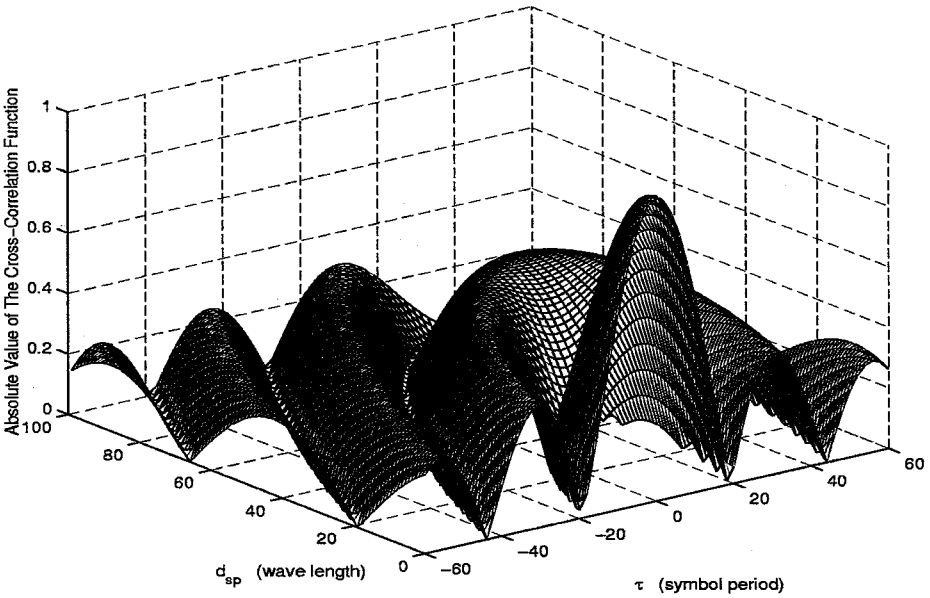

Fig. 2. 3-D plot of magnitude of the cross-correlation function for $d = 1000\lambda$, $a = 25\lambda$, $\beta = \pi/6$, $\xi = 7\pi/12$, and $f_D T = 0.02$.

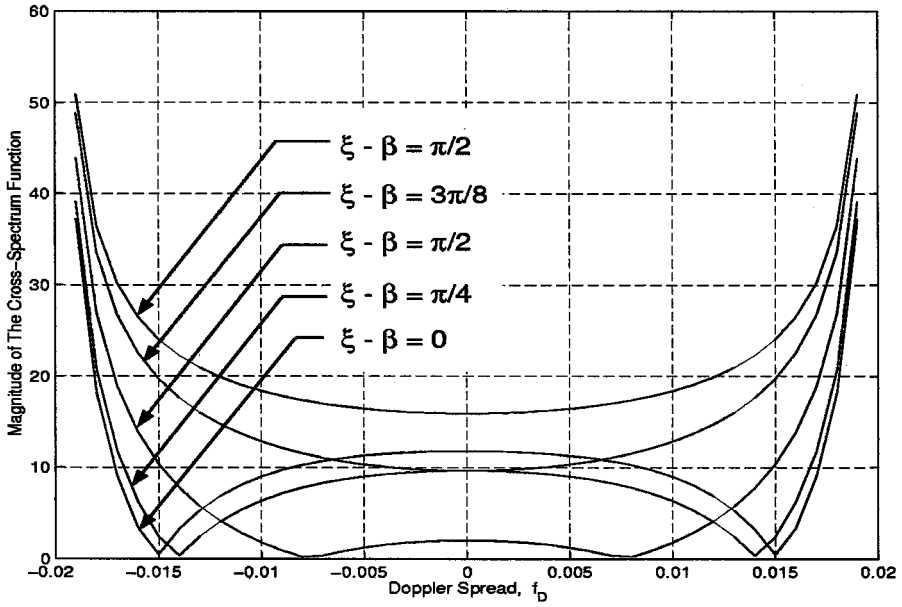

Fig. 3. Cross-spectrum corresponds to different mobile moving directions. The parameters are the same as Fig. 2 and $d_{sp} = 30.6\lambda$.

ID design is to choose the minimal (space only) optimal AS first and then the ID is identified to give the desired overall operating point. This methodology is optimal for the situation where AS design is more constrained than ID (i.e., packet data at relatively low carrier frequencies). Obviously selecting ID first might be a more appropriate methodology in other applications (i.e., voice at high carrier frequencies). To this end, we first investigate the AS design with the help of the proposed channel model to predict the performance. The channel model presented in Section II is parametric in several geometries. The goal of this section is to optimize performance for a given set of geometries and explore the amount of degradation experienced for closely spaced antennas. In contrast to other results [3]–[7], we examine the binary phase shift keying (BPSK) system bit error probability (BEP) performance. The details of the pairwise error probability calculation over correlated fading channels with perfect CSI are presented in Appendix II.

The AS design is a demonstration of an application with the proposed model. Although the phenomenon revealed in this work is consistent with predictions of the previous work, the investigation helps in gaining intuition for the model and its application on space-time modems in the later discussion. Additionally, using the BEP performance gives a more specific E_b/N_0 characterization of the design tradeoffs and directly reflects the power efficiency.

To examine the effects of AS, we need to specify an acceptable correlation value. For sake of simplicity of understanding the methodology, we choose for this discussion the first zero of the Bessel function as our design point. Any other correlation value can be selected and the following design procedure

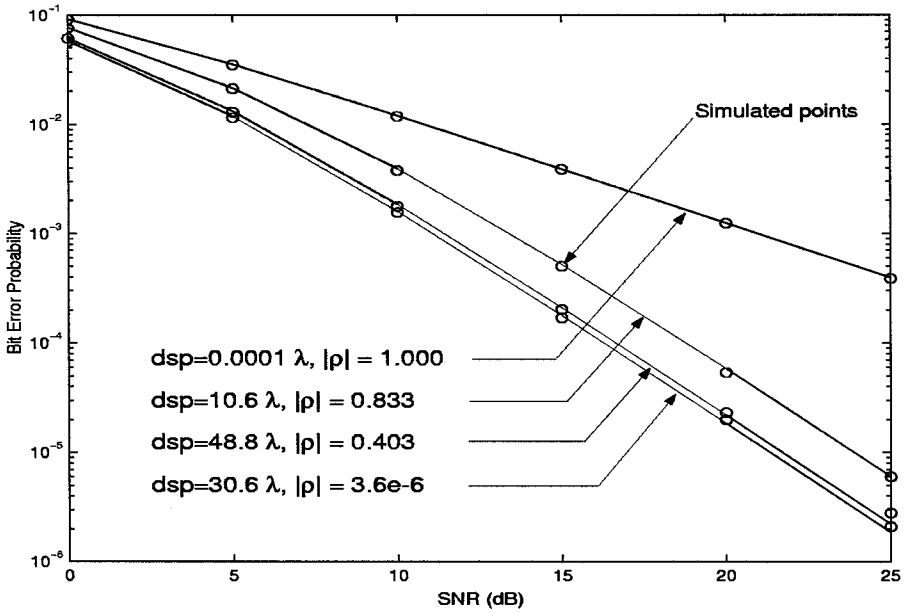

Fig. 4. BPSK BEP under the parameter set of $\tau = 0$, $a_\lambda = 25$, $d_\lambda = 1000$, and $\beta = \pi/6$.

would be applicable. To derive the optimal AS, apply the approximation (36) and (37) derived in Appendix I in the function $R_{c_1c_2}(0, d_{sp})$. After simplification, the argument in the Bessel function becomes

$$\frac{2\pi a}{\lambda d}\, d_{sp} \sin\beta. \tag{7}$$

Since the first null of the Bessel function, which ensures independent fading between the received signals, occurs when its argument equals to 2.40483, the smallest optimal AS can be obtained as

$$\frac{d_{sp}}{\lambda} = k_1 \frac{d_\lambda}{a_\lambda \sin\beta} \tag{8}$$

where $k_1 = 2.40483/2\pi$ is a constant, and $d_\lambda = d/\lambda$ and $a_\lambda = a/\lambda$ denote wavelength normalized parameters.

It can be seen that a larger AS is required to ensure independent fading between received signals of a snapshot for a lower carrier frequency, longer mobile distance, smaller scatterer ring radius, or smaller mobile position angle. The Doppler frequency and the mobile moving direction, on the other hand, do not affect the AS design. Note that the mutual coupling effect between antennas is ignored, and hence when AS is smaller than half of a wavelength, the system performance demonstrated is only conceptual.

We now consider the case where $\tau = 0$, $\beta = \pi/6$ (corresponding to a three-sector cellular tower configuration), $a_\lambda = 25$, and $d_\lambda = 1000$ (corresponding to 2.9° of multipath angular spread). Note that the first null of the cross-correlation function occurs when $d_{sp} = 30.6\lambda$, and the maximum $(\rho = 0.403)$ for $d_{sp} > 30.6\lambda$ occurs at the second lobe when $d_{sp} = 48.8\lambda$. The performance of BPSK modulation is shown in Fig. 4 for $d_{sp} = 0.0001\lambda$, 10.6λ, 30.6λ, and 48.8λ. Included in this plot are simulations of the model to verify the validity. In the simulation, the ring of scatterers was modeled with 50 individual scatterers uniformly distributed on the ring, and no approximation or far field assumption was used to compute the propagation phase offsets. Note that the signal-to-noise ratio (SNR) is defined according to the transmitting power. Hence, the receiver diversity system will have an intrinsic gain of 3 dB over a single receiving antenna system of the same diversity level.

Referring to Fig. 4, at $d_{sp} = 0.0001\lambda$, the system is almost equivalent to receiving the same signal twice, but without doubling the transmitting power. Strong correlation between these two received signals makes them suffer essentially the same fading, and no diversity is gained. At $d_{sp} = 30.6\lambda$, the received signal pair is independent, and the system achieves full diversity. As d_{sp} increases further to the second lobe maximum, the BEP increases, but does not have a significant change ($\leq$0.5 dB). Hence, AS corresponding to the first null of the Bessel function is a reasonable choice for the acceptable minimum AS. Again, a smaller AS which corresponds to another point on the Bessel function could be chosen as the minimum AS and the whole discussion would still be valid.

The effect of model parameters is similar to that documented in [7]. In general, channels become more correlated with smaller angular spread or as the mobile moves toward the end-fire position of the two antennas. Once the AS is optimized for a certain scenario, the BEP performance will not have a significant variation ($\leq$0.5 dB) if the mobile moves to a location of smaller channel correlations. Extensive numerical results for this receiver diversity study are presented in [8].

It is quite likely that space limitations at the BS will prevent achieving the independent fading. The degradation due to a smaller AS than the optimal one is demonstrated here by first finding the optimal AS for a set of parameter, and then reducing the AS until it causes 1 and 3 dB of pairwise SEP degradation when SNR is 20 dB. The same parameter set as the previous part is selected, and one parameter is examined at a time.

A study of the allowable separation for BS antennas while achieving a prescribed performance was completed. Fig. 5

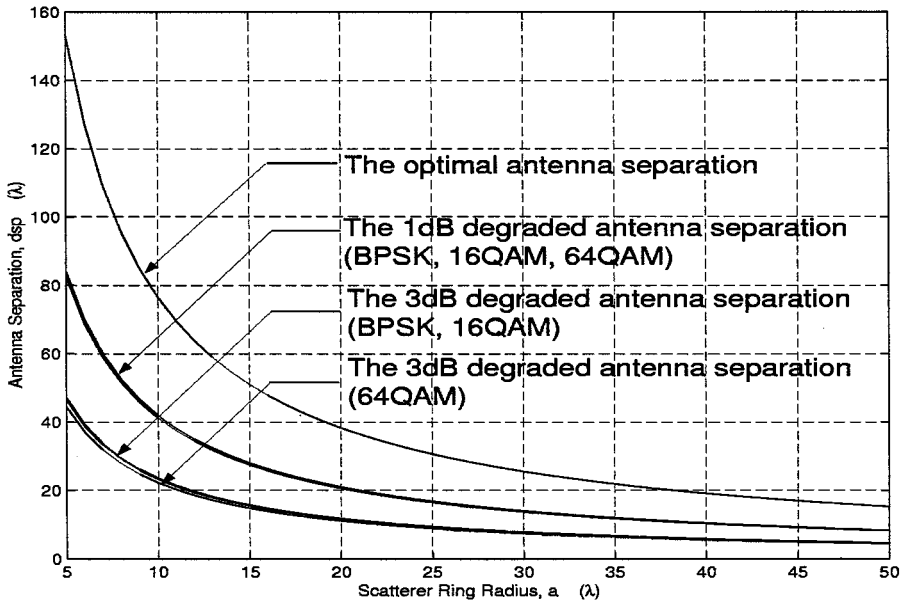

Fig. 5. The optimal, 1 and 3 dB of pairwise SEP degraded antenna separations with respect to a_λ. $d_\lambda = 1000$ and $\beta = \pi/6$.

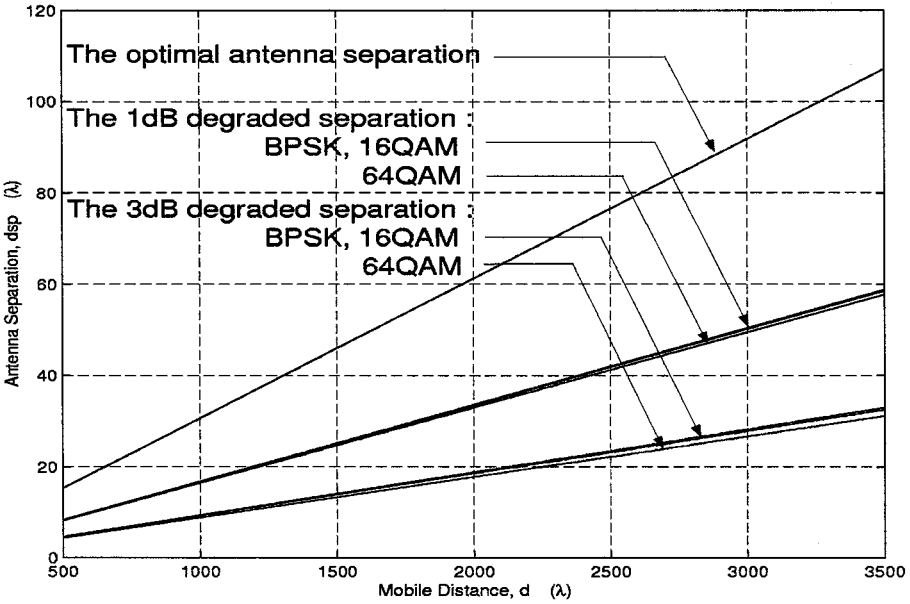

Fig. 6. The optimal, 1 and 3 dB of pairwise SEP degraded antenna separations with respect to d_λ. $a_\lambda = 25$ and $\beta = \pi/6$.

shows the allowable antenna separation for 1 and 3 dB degradations as a function of the scatterer ring radius for $d_\lambda = 1000$ and $\beta = \pi/6$. Likewise, Figs. 6 and 7 document the same results as a function of the mobile distance and the mobile position angle. Note that although the spatial correlation is not a linear function of a_λ, d_λ, or $\sin(\beta)$ (see Appendix I), and the SEP performance is a fairly complicated function of the spatial correlation (see Appendix II), the SEP curves demonstrated in Figs. 5–7 appear to be approximately linear in d_λ and approximately inverse-linear in a_λ and $\sin(\beta)$. A closer examination of the cross-correlation function (the Bessel function) and the SEP expression in the region considered can confirm this dominant characteristic. Numerical computation, however, is necessary to precisely characterize each parameter's influence on the system performance. It is seen that approximately 1 dB of pairwise SEP degradation will be caused if the AS is reduced to 1/2 of its optimal separation, and approximately 3 dB of pairwise SEP degradation will be caused if it is reduced to 1/3 of its optimal separation. The constellation size only has a slight effect on the degraded AS. Also seen in these figures is that the gap between curves is smaller when the optimal AS is smaller. This means that the system is more sensitive in the absolute-quantity sense to the AS selection when the optimal AS is small.

It has been shown in [7] and [8] that the degradation caused by the variation of geometric parameters d and a is not significant unless the mobile is in a rare environment (e.g., driving far away from the base station, or entering a garage). The parameter β, however, has a large impact on a system's performance especially when it is near zero (i.e., mobile at the end-fire location). The situation can be improved if more than two antennas are

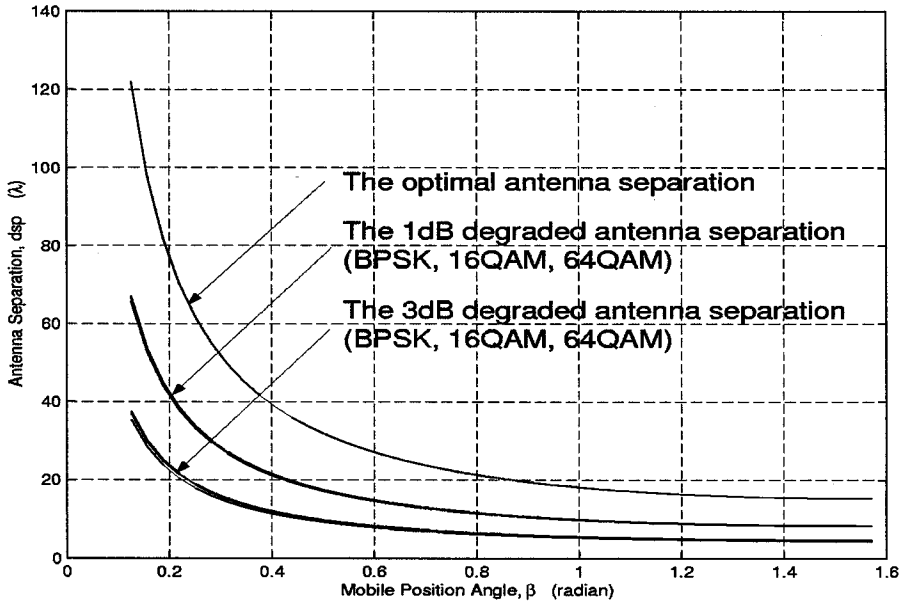

Fig. 7. The optimal, 1 and 3 dB of pairwise SEP degraded antenna separations with respect to β. $d_\lambda = 1000$ and $a_\lambda = 25$.

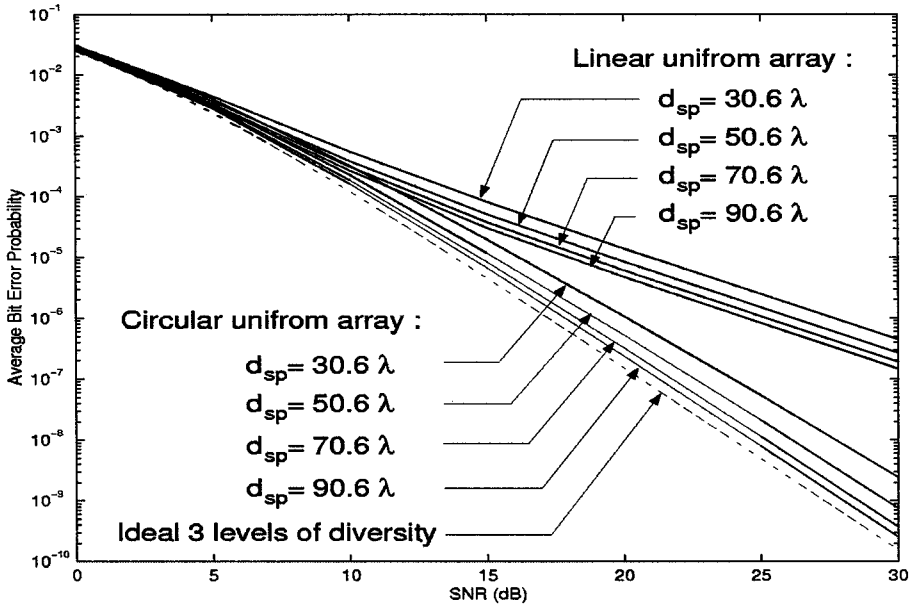

Fig. 8. Average BPSK BEP of 3 receiving antennas, linearly and circularly placed, with respect to d_{sp}. $a_\lambda = 25$ and $d_\lambda = 1000$.

available. Two possible multiple-antenna placements are linear uniform arrays (LUA) and circular uniform arrays (CUA).

Under the assumption of β being uniformly distributed on $[0, 2\pi]$, the average pairwise SEP can be expressed as

$$E\{P_{d_i}\{d_i \to d_j\}\} = \frac{1}{2\pi}\int_0^{2\pi} P_{d_i}\{d_i \to d_j \,|\, \beta\}\, d\beta \qquad (9)$$

where $P_{d_i}(d_i \to d_j)$ is the pairwise SEP of decoding d_i over d_j given d_j transmitted.

No analytical solution is available for evaluating the integral. However, due to the bounded and continuous nature of the integrand, the numerical Riemann sum approximation can be applied.

In general, the CUA ensures that not all antennas are in a highly correlated situation like what can happen with an LUA when $\beta = 0$, and consequently gives the better average performance. This average performance improvement for three antennas is shown in Fig. 8; [8] provides further results.

IV. Joint Space-Time Demodulation

This section will investigate how the physically motivated space-time model of this paper affects the performance of a space-time modem architecture. This investigation will consider the simplest system possible to gain intuition: an uplink (mobile to base) with a simple interleaved (interleaving depth τ_{dep}) BPSK repetition code (rate = 1/2) and dual antenna receiver diversity. An illustration of such a system is shown in Fig. 9. One of the most significant motivators for space-time modems is that the potential diversity achieved in a space-time

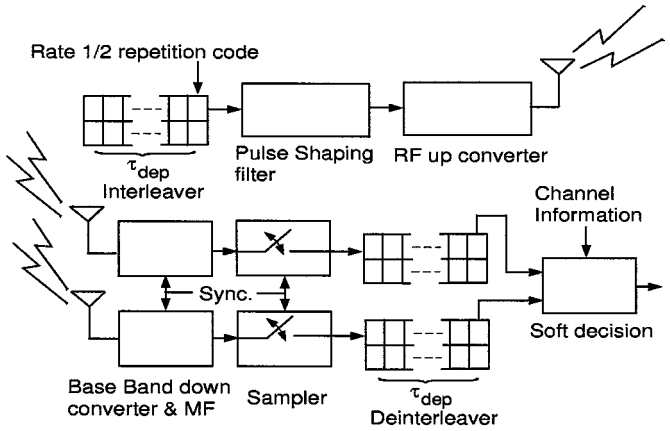

Fig. 9. A joint time and receiver diversity system with each individual diversity equal 2.

modem is expected to be the product of the number of diversity levels achieved in each of the space and time dimension. Consequently, it should provide ideally four levels of diversity in our simplest system. Understanding how the maximal level of diversity can be achieved in this simplest system will provide a great deal of insight into more complicated space-time modem architectures.

A. Diversity Characteristics of Space-Time Demodulation

Spatial-temporal correlations often produce counterintuitive behavior in a space-time system. There are two important properties for time diversity coding with multiple receiving antennas. First, having optimal AS in space and optimal ID in time does not guarantee a low BEP (i.e., that four levels of diversity are obtained). To demonstrate this characteristic, we examine the case where $d_\lambda = 1000$, $f_D T = 0.02$, and $d_{sp} = 30.6\lambda$. It can be shown in this case with $a_\lambda = 25$ and $\tau_{dep} = 19.1T$, the AS will generate instantaneous spatially independent channels and for each spatial channel the ID provides independent time diversity. However, the channel is highly correlated jointly across space and time, and hence the BEP is degraded. Only three levels of diversity are observed. Fig. 10(a) shows this characteristic for $\beta = \pi/6$ and $\xi = 2\pi/3$. Second, increasing ID does not necessarily improve the performance, as it usually does in a time-only diversity system. To demonstrate this, consider the same case as above except with $a_\lambda = 30$, $\beta = \pi/2$, and $\xi = \pi$. Fig. 10(b) and (c) show that an ID $\tau_{dep} = 19.1T$ gives almost an ideal four levels of diversity, while $\tau_{dep} = 43.9T$ results in only an approximate three levels of diversity. This performance difference can be as large as 4 dB when the SNR is 30 dB. The reasons for these counterintuitive results will be examined in the sequel.

Let's use the simple example considered here to clarify the notion of achieving diversity in a space-time system. Let $r_1(t_1)$, $r_2(t_1)$ denote received symbols at each antenna at time t_1, and $r_1(t_2), r_2(t_2)$ at time t_2. Note that in our simple repetition code system, if the transmitted symbol was d_i, then $r_k(t_m) = \sqrt{E_s} d_i c_k(t_m) + n_k(t_m)$, where E_s is the transmitted symbol energy, c_k is the fading channel distortion, n_k is the additive white Gaussian noise, subscript k corresponds to the antenna ordering, and t_m is the time index. To get full diversity means having four nearly independent fading channel distortions, which require six pairwise independence conditions. The joint AS and ID design corresponds to finding an operating point corresponding to the arguments of the function $R_{c_1 c_2}(\tau, d_{sp})$ that gives as many near independent pairs as possible.

A plot of the constant correlation contours of $R_{c_1 c_2}(\tau, d_{sp})$ can provide significant insight into the space-time characteristics of this model. Fig. 11 shows the contour plot of $R_{c_1 c_2}(\tau, d_{sp})$ with $d_\lambda = 1000$, $a_\lambda = 25$, $\beta = \pi/6$, $\xi = \pi/2$, and $f_D T = 0.02$. This is a 2-D representation of a figure having a form much like Fig. 2. Note that $R_{c_1 c_2}(\tau, d_{sp})$ depends only on f_D at the τ-axis ($d_{sp} = 0$), and depends only on the model parameters on the d_{sp}-axis ($\tau = 0$). The space-time operating point is defined to be the vertices of the rectangle anchored at (0, 0) with length τ_{dep} along the τ-axis and length d_{ant} along the d_{sp}-axis.[1] The three nonzero vertices define the six pairwise correlations that are important [time-only correlation (two pairs), space-only correlation (two pairs), and space-time correlation (two pairs)]. Referring to Fig. 11, every operating point on line L projects to a null on the τ-axis, and hence guarantees that the received symbols on each individual antenna will experience independent fading if separated in time by this depth. The situation is shown pictorially on the central diagram of the bottom of Fig. 11 where symbols circled by an oval indicate the independence between them. The same description applies on line H (independence across antennas at the same time) and all null contours (independence across both space and time). Note the contour plotted here helps explain the situation described earlier in Fig. 10(a) where the selected operating point O, whose coordinate is $(\tau_{dep}, d_{ant}) = (19.1T, 30.6\lambda)$, corresponds to a point of high space-time correlation (and hence only three levels of effective diversity). Similarly, the cases presented in Fig. 10(b) and (c) represent the case where the space-time operating point moved from a region of low correlation to one of high correlation.

B. Achieving Full Diversity

The goal of full diversity can be achieved if the operating point of the space-time modem lies outside the high cross-correlation region. The shaded area R_U in Fig. 11 is the union of the area inside the first null contour $R_N(\xi - \beta)$, whose region depends on $(\xi - \beta)$, and the points having projections smaller than the first null on the d_{sp}-axis or τ-axis denoted as R_L and R_H, respectively.[2] Having the operating point of a space-time modem lie in this area will reduce the level of diversity and hence should be avoided when designing AS and ID. Note that the discussion in the previous section can be extended to explain that the maximal channel correlation outside R_U is only 0.4, and will not cause significant system degradation. The choice of ID and AS to avoid being in R_L and R_H is well understood [3], [4], [6], [7]. Consequently, in addition to these design rules, the design cri-

[1]It is more accurate to specify an operating point as a pair, as both (τ_{dep}, d_{ant}) and $(-\tau_{dep}, d_{ant})$ are involved in contributing the diversity gain. However, due to the symmetric behavior of the cross-correlation with respect to $\xi - \beta$, (τ_{dep}, d_{ant}) is sufficient to characterize the system performance if we limit $\xi - \beta$ to be in $[0, \pi]$.

[2]Just as described earlier, we have chosen the first null contour of the Bessel function as our design region, although any other contour could be selected and the following design procedure would be applicable.

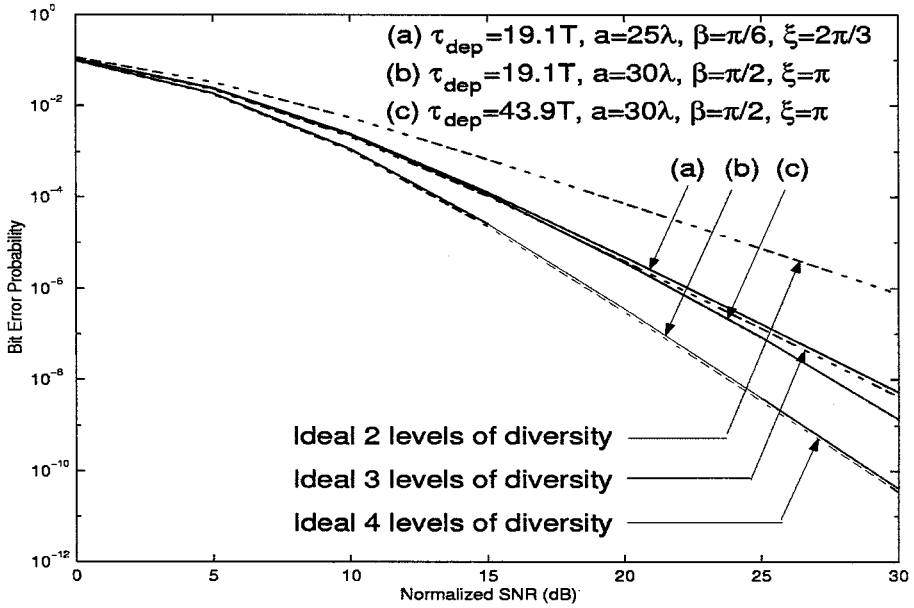

Fig. 10. Illustrations of situations not achieving full diversity. $d_\lambda = 1000$, $f_D T = 0.02$, and $d_{sp} = 30.6\lambda$ are the same for all cases.

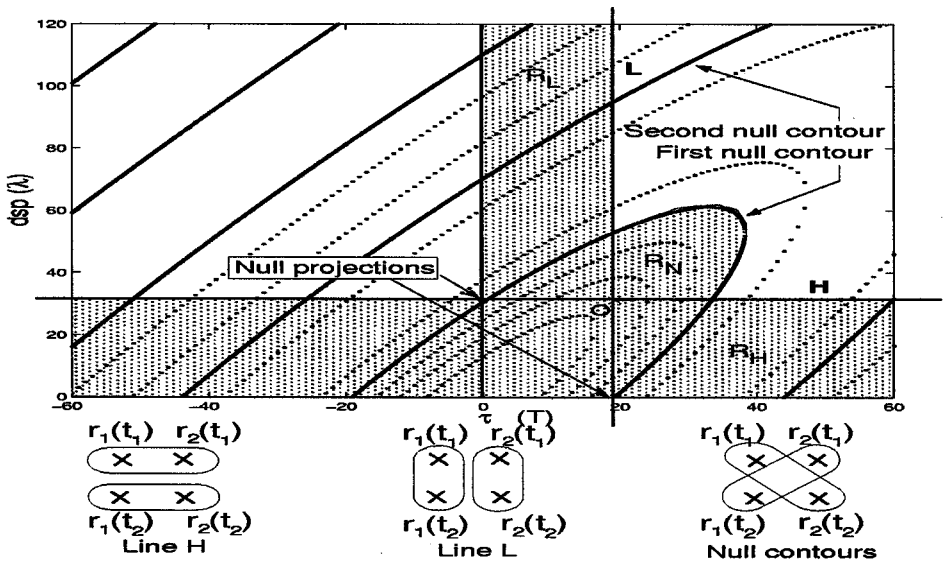

Fig. 11. Space-time cross-correlation function contour plot for $f_D T = 0.02$, $a_\lambda = 25$, $d_\lambda = 1000$, $\beta = \pi/6$, and $\xi = \pi/2$. The bottom 3 diagrams show pictorially symbol independence.

teria postulated in this section are mainly their generalizations on the space and time interactive region $R_N(\xi - \beta)$.

This section will consider a wireless network where the propagation geometry will vary within each sector of interest. To ensure that an operating point (τ_{dep}, d_{ant}) lies outside R_H, it must satisfy

$$d_{ant} \geq d_{a.d.} = k_1 \frac{d_{\lambda \max}}{a_{\lambda \min} \sin \beta_{\min}} \tag{10}$$

where subscript $a.d.$ is an abbreviation for "antenna diversity," and $\max$ and $\min$ denote the maximum or minimum of the corresponding parameters within each sector of interest. Likewise, the operating point will lie outside R_L when τ_{dep} satisfies

$$\tau_{dep} \geq \tau_{t.d.} = \frac{k_1}{f_D} \tag{11}$$

where subscript $t.d.$ is an abbreviation for "time diversity." Consequently, two necessary conditions for a space-time system to achieve full diversity over the sector of interest are $\tau_{dep} \geq \tau_{t.d.}$ and $d_{ant} \geq d_{a.d.}$.

The calculation whether an operating point lies in $R_N(\xi - \beta)$ is a bit more complicated. We start with the slope computation of every point on the correlation contours, which can be obtained by computing the ratio of the partial derivatives as

$$-\frac{\partial R_{c_1 c_2}(\tau, d_{sp})/\partial \tau}{\partial R_{c_1 c_2}(\tau, d_{sp})/\partial d_{sp}} = -\frac{d^2 \lambda^2 f_D^2 \tau + a d \lambda \sin\beta \sin(\beta - \xi) f_D d_{sp}}{a d \lambda \sin\beta \sin(\beta - \xi) f_D \tau + a^2 \sin^2 \beta d_{sp}} \tag{12}$$

where the approximations of (36) and (37) have been used to simplify the expression. It is observed that when $\xi = \beta$, the

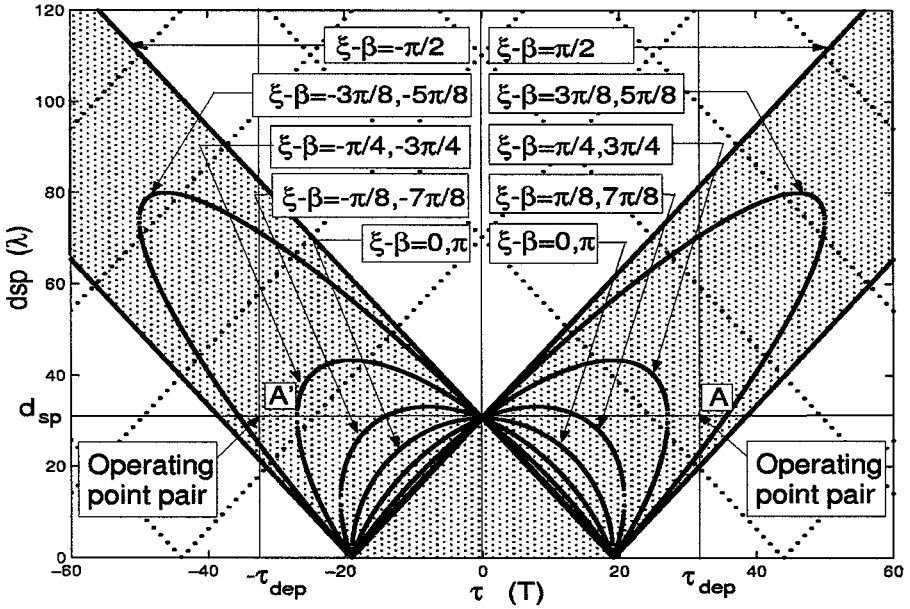

Fig. 12. Space-time cross-correlation function first null contours corresponding to various $(\xi - \beta)$'s. $f_D T = 0.02$, $d_\lambda = 1000$, $a_\lambda = 25$, and $\beta = \pi/6$ are used for all cases.

contours are all vertical on the τ-axis and all horizontal on the d_{sp}-axis. This implies that the main lobe of $R_{c_1c_2}(\tau, d_{sp})$ would be contained within the intersection of R_L and R_H, and an operating point will achieve full diversity if both of the spatial and temporal diversity is achieved.

For situations when $\xi \neq \beta$, the characterization of an operating point becomes a bit more complicated. Referring to Fig. 12, as ξ increases, the contours start to stretch out until $\xi = \beta + \pi/2$ where all contours become parallel with slope equal to $(f_D \lambda d_\lambda / a_\lambda \sin\beta)$. The parallel contour is considered the worst case due to the unbounded nature of $R_N(\xi - \beta)$. The same observation can be seen in (4) that when $\xi = \beta + \pi/2$, the cross-spectrum (and hence the cross-correlation) is maximized. The cause of this phenomenon is that the phase offset increment caused by the Doppler frequency (in time domain) happens to cancel the phase offset increment caused by the propagation delay (in space domain) for every scatterer when the mobile moves tangentially to the BS. The same correlation is hence preserved if both time and space are increased at the same time. In the less uniform scattering environment encountered in practice, the high cross-correlation region may not be unbounded, but a long high cross-correlation region can still be expected. If ξ keeps increasing until it equals $\beta + \pi$, the contours shrink and tilt to the negative τ-axis. The symmetric behavior applies when ξ passes $\beta + \pi$ and keep increasing till $\xi = \beta + 2\pi$. Due to the obvious symmetry, we can just focus on the case of $\xi \in [\beta, \beta + \pi/2]$.

Recall the characteristics of $R_N(\xi - \beta)$ are a function of d_{ant}, β, a_λ, d_λ, ξ, and f_D. Since the channel geometric parameters have similar effect on the performance, we define a new parameter $\gamma(d_{ant}, \beta, a_\lambda, d_\lambda)$ to combine them:

$$\gamma(d_{ant}, \beta, a_\lambda, d_\lambda) \triangleq \frac{d_{ant}}{d'_{ant}} \tag{13}$$

where $d'_{ant} \triangleq k_1(\lambda d_\lambda / a_\lambda \sin\beta)$ is the nominal optimal AS for the given geometry of the mobile. Note that the AS d_{ant} is a fixed value which is obtained by substituting the specified extreme values of parameters into (10), while the nominal AS d'_{ant} is varying with respect to different mobile locations. For notational simplicity, arguments of the function $\gamma(\cdot)$ will be ignored in the sequel. Note that with antenna separation such that ideal space diversity is achieved [see (10)], γ is always greater than one. The performance of a space-time system is now viewed as a being a function of f_D, $\xi - \beta$, and γ.

For a selected operation point (τ_{dep}, d_{ant}), two open questions now are apparent.

1) What are the range of values of γ that could cause an operating point to lie in $R_N(\xi - \beta)$?
2) For a given γ that is potentially in $R_N(\xi - \beta)$, what is the probability that the mobile moving direction would cause the operating point to lie in $R_N(\xi - \beta)$? And what is the maximum of this probability (the worst case) with all potentially "bad" values of γ considered?

The answers to these two questions provide a method to characterize a selected operation point. This will also be applied in the discussion of the ID design in the sequel.

To answer the first question, rewrite the argument of the Bessel function in (3) for a given $\xi - \beta$, and f_D to obtain an inequality describing $R_N(\xi - \beta)$ as

$$f_D^2 \tau_{dep}^2 - 2 f_D \tau_{dep} k_1 \gamma \sin(\xi - \beta) + k_1^2 \gamma^2 < k_1^2. \tag{14}$$

The inequality can be rewritten as

$$\sin(\xi - \beta) > g(\gamma, \tau_{dep}) > 0 \tag{15}$$

where

$$g(\gamma, \tau_{dep}) = \frac{k_1^2(\gamma^2 - 1) + f_D^2 \tau_{dep}^2}{2 f_D \tau_{dep} k_1 \gamma}. \tag{16}$$

Note that if (τ_{dep}, d_{ant}) and all other parameters satisfy (14) [in other words, validate (15)], the (τ_{dep}, d_{ant}) will be inside $R_N(\xi-\beta)$. The only possibility for (15) to be valid for some $\xi-\beta$ is when $g(\gamma, \tau_{dep})$ is less than one. Solving for the inequality $g(\gamma, \tau_{dep}) \leq 1$ gives the range of γ, denoted as R_γ, that may cause the operating point (τ_{dep}, d_{ant}) to lie in $R_N(\xi-\beta)$ for a given $f_D\tau_{dep}$. This range is derived as

$$R_\gamma(\tau_{dep}) = \left\{ \gamma \in [\gamma_l, \gamma_u] \,|\, \gamma_l = \max\left(1, -1 + \frac{f_D\tau_{dep}}{k_1}\right) \right. \\ \left. \gamma_u = 1 + \frac{f_D\tau_{dep}}{k_1} \right\} \tag{17}$$

The case that $\gamma \in R_\gamma$ does not necessarily imply poor performance. The operating point A in Fig. 12 where $R_\gamma(\tau_{dep}) = [1, 2.72]$ and $\gamma = 1$ serves as a good example. It is seen that when $\xi - \beta = \pi/4$, this operating point is not in the high correlation region, and the system will still perform well. Consequently, answering the second question above will go a long way toward assessing the performance of a given operating point.

The desired probability is obtained by first noting that if $\xi = \xi_0 + \beta$ satisfies the inequality (15), so will every $\xi \in [\xi_0 + \beta, \pi/2 + \beta]$ (recall that $\xi \in [\beta, \beta + \pi/2]$), and, as described earlier, the operation point will be in $R_N(\xi - \beta)$ for these $(\xi - \beta)$'s because altogether they validate (15). The probability that $R_N(\xi - \beta)$ covers the operating point when $\gamma \in R_\gamma$, which is denoted $q(\tau_{dep}, \gamma)$, is given as

$$q(\tau_{dep}, \gamma) = 1 - \frac{2}{\pi} \sin^{-1}(g(\gamma, \tau_{dep})). \tag{18}$$

$q(\tau_{dep}, \gamma)$ gives a probability of bad performance with respect to a single $\gamma \in R_\gamma(\tau_{dep})$. The maximum probability (the worst case probability) for all $\gamma \in R_\gamma(\tau_{dep})$ can be further derived to provide a quick characterization on how good the performance is guaranteed to be with a selected ID. The maximum probability of "bad" mobile moving direction occurs when $\xi - \beta$ is minimum and still satisfies (15). The corresponding $\xi_{\min}$ can be found by solving the equation $(dg(\gamma, \tau_{dep})/d\gamma) = 0$. Then substitute the answer, which is $\gamma = \max(1, \sqrt{(f_D\tau/k_1)^2 - 1})$ (after considering its suitable range), back into (15). The maximal probability that $R_N(\xi - \beta)$ covers the operating point is therefore

$$q_{\max}(\tau_{dep}) = \begin{cases} 1 - \frac{2}{\pi} \sin^{-1}\left(\sqrt{1 - \left(\frac{k_1}{f_D\tau_{dep}}\right)^2}\right) & \text{if } \frac{f_D\tau_{dep}}{k_1} \geq \sqrt{2} \\ 1 - \frac{2}{\pi} \sin^{-1}\left(\frac{f_D\tau_{dep}}{2k_1}\right) & \text{otherwise.} \end{cases} \tag{19}$$

With (17) and (18), for a given (τ_{dep}, d_{ant}), we can decide the range of γ which may degrade the system, and for each value of γ the probability that the system is degraded; (19) further gives the maximal probability of degraded performance for all $\gamma \in R_\gamma(\tau_{dep})$.

V. Design for Space-Time Modems

One of the goals in a modeling effort as in this paper is to come up with some design rules for AS and ID that will provide good average performance for space-time modems. In this section we try to use our model to formulate these design rules. The level of success of these design rules can only be validated with extensive field trials.

As described earlier, in our approach to joint AS and ID design, the AS is selected first and then the ID is chosen to complete the selection of an operating point (τ_{dep}, d_{ant}). Again, as the two necessary conditions described earlier, d_{ant} must be chosen to be greater than $d_{a.d.}$ and τ_{dep} must be checked to ensure that it is greater than $\tau_{t.d.}$. The selected d_{ant} together with all possible mobile location parameters decide the range of the parameter γ [defined in (13)]. Generally speaking, a larger ID is required for a larger value of γ to ensure the full diversity. In our design, we only focus on the design which would benefit the system as far as the diversity performance is concerned. For some situations, a mobile can be in a better communication location where the γ, and hence the required ID, is still very large. For example, when the mobile moves closer to the base station, the value of γ increases, which means a larger ID is required for maintaining the same diversity level. However, when the mobile moves closer to the base station, a higher SNR is expected and better performance of algorithms may be achieved, which would improve the system even though the required ID is larger. Hence, a careful design should take all the benefits of diversity gain and other issues into account, and decide how to apply the diversity gain to compensate for a worst case transmission scenario.

To design a good operating point, we focus on two possible designs: a design based on the worst case (min-max procedure) and a design that works well on average. In both designs, the AS is fixed while the ID is explored. The worst case design, although providing a prescribed performance for all scenarios, requires a much larger ID. The average design does not guarantee full diversity in all instances but requires a smaller ID and works well on average.

A. The Worst-Case Design

The worst-case occurs whenever $\beta = \xi + \pi/2$, in which case the slope on the contour becomes $(f_D\lambda d_\lambda/a_\lambda \sin\beta)$ or $f_D d'_{ant}/k_1$ everywhere. This means the high cross-correlation area, $R_N(\xi - \beta)$, becomes a strip, and its boundary intercepts the positive τ-axis at $\tau_{t.d.}$ and the positive d_{sp}-axis at d'_{ant}. Note that a smaller slope corresponds to a larger γ when AS is fixed.

Under the worst-case scenario, it is easy to show by linear algebra that for $(d_{ant}, \tau_w) \notin R_N(\xi - \beta)$, d_{ant} and τ_w must satisfy the inequality

$$\left| k_1 \frac{d_{ant}}{d'_{ant}} - f_D\tau_w \right| \geq k_1 \tag{20}$$

where τ_w indicates the ID for the worst-case scenario.

The inequality (20) suggests switching ID between two preselected values depending on the mobile's location and speed, which is practically unattractive. If an approximate range of these parameters is known, a simpler design using a single ID

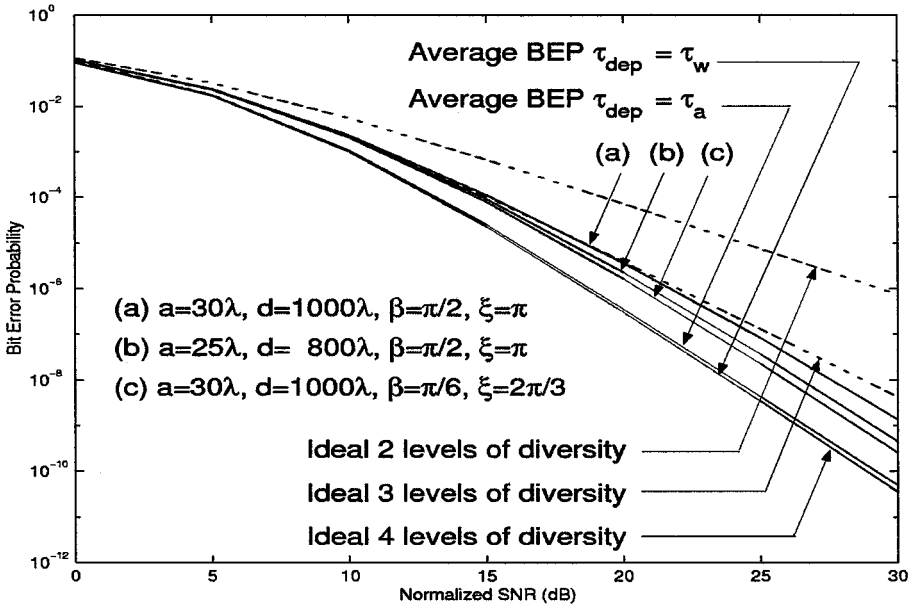

Fig. 13. Average BEP of using τ_a and τ_w, and examples of possilbe poor performance with τ_a. $f_D T = 0.02$, $d_{ant} = 30.6\lambda$ are fixed for all cases.

can be obtained by focusing on one side of the inequality (20) only.

The side of the inequality (20) that upper bounds τ_w does not guarantee a good solution. This can be easily seen when the mobile is at the location achieving the optimal AS (i.e., $d'_{ant} = d_{ant}$) the only possible solution is $\tau_w = 0$, which will not give high diversity level. Focusing on the side that gives lower bound for τ_w and simplifying it, we have

$$\tau_w \geq \tau_{t.d.} + \frac{k_1 \gamma_{\max}}{f_D} = \tau_{t.d.}(1 + \gamma_{\max}). \tag{21}$$

The inequality dictates that $(1 + \gamma_{\max})$ times larger ID than a single time diversity system will be required for the worst case design. The parameter γ [defined in (13)], and therefore the required ID, is usually smaller when the mobile moves closer to the cell edge where the diversity gain plays a more important role due to the lower SNR. This observation renders the possibility of characterizing $\gamma_{\max}$ and the required ID according to a system link budget. The performance achieved by higher SNR or that by diversity gain can hence be balanced according to the requirement of a design.

As a design example, consider the set of parameters that $f_D T = 0.02$, $a_\lambda = 25$, $d_\lambda = 1000$, and $\beta = \pi/6$. The corresponding optimal AS is $d_{a.d.} = 30.6\lambda$ and is chosen to be the AS, i.e., $d_{ant} = d_{a.d.} = 30.6\lambda$. Assume that $\gamma_{\max} = 20$, for which one possible combination of geometric parameter ranges is $a_\lambda \leq 50$ and $d_\lambda \geq 200$ ($\sin\beta$ contributes a factor of 2). The required ID must then be bigger than $401.9T$, while only $19.1T$ is required for a single time diversity system. To make sure the projection on the τ-axis is a null, an ID of $418.8T$ is chosen.

The unsafe range R_γ of γ can be computed by applying (17) from which we obtain that $(1, \gamma_{\max}) \cap R_\gamma = \emptyset$. This means the ID ensures the operating point will never be in $R_N(\xi - \beta)$ as long as $\gamma \leq \gamma_{\max}$. In characterizing the performance, the BEP is averaged over $25 \leq a_\lambda \leq 50$ with resolution 5, $200 \leq d_\lambda \leq 1000$ with resolution 50, $\pi/6 \leq \beta \leq 5\pi/6$ with resolution 5°, and $0 \leq \xi < 2\pi$ with resolution 5°, and shown in Fig. 13. Note that equal steps are taken in averaging over a_λ and d_λ for simplicity, although they are not likely to be uniformly distributed. Also, some power control mechanism is assumed so that the received signal power does not vary with respect to d_λ. The average BEP performance of using (d_{ant}, τ_w) as the operating point is indistinguishable from the ideal maximal diversity curve and hence has a near-full diversity performance. There will only be a slight variation for all instances satisfying the design scenario.

B. The Average Design

The region $R_N(\xi - \beta)$ is a function of the mobile moving direction ξ and the parameter γ [defined in (13)], which accounts for the parameters associated with the link geometry. The average ID design will average the minimal optimal ID, $\tau_{\text{opt}}(\xi, \gamma)$, over ξ for a given γ. The worst situation average ID (occurred when $\gamma \to \infty$) is then chosen as the design ID. This design will assume that ξ is uniformly distributed. This procedure greatly reduces the ID used but results in some situations where full diversity is not achieved.

To understand this design, we first need to identify the minimal optimal ID as a function of both γ and ξ. Note for a given γ, a threshold ξ_{th} exists such that when $\xi \leq \xi_{th}$, the horizontal line $d_{sp} = d_{ant}$ on the contour plot does not intercept the region $R_N(\xi - \beta)$. When $\xi \leq \xi_{th}$, the region $R_N(\xi - \beta)$ is contained within R_H and the minimal optimum ID is $\tau_{t.d.}$. On the other hand, when $\xi > \xi_{th}$, the horizontal line $d_{sp} = d_{ant}$ intercepts $R_N(\xi - \beta)$, and the right intercepting point should be selected as the operating point. The threshold ξ_{th} can be computed by solving the simultaneous equations

$$\begin{cases} f_D \tau = k_1 \gamma \sin(\xi - \beta) \\ f_D^2 \tau^2 - 2 f_D \tau k_1 \gamma \sin(\xi - \beta) + k_1^2 \gamma^2 = k_1^2 \end{cases} \tag{22}$$

where the first equation comes from zero slope of (12) and the second equation represents the first null contour. The solution is obtained as $\xi_{th} = \beta + \cos^{-1}(1/\gamma)$.

The minimal optimal interleaving depth can then be expressed as

$$\tau_{\text{opt}}(\xi,\gamma)=\begin{cases}\dfrac{k_1}{f_D} & \text{if } \beta\le\xi\le\beta+\cos^{-1}\dfrac{1}{\gamma}\\ \dfrac{k_1}{f_D}\left(\gamma\sin(\xi-\beta)+\sqrt{1-\gamma^2\cos^2(\xi-\beta)}\right) & \\ & \text{if } \beta+\cos^{-1}\dfrac{1}{\gamma}<\xi\le\beta+\dfrac{\pi}{2}.\end{cases}$$

For computational simplification, we assume $\gamma\ge\sqrt{2}$ so that when $\xi\ge\xi_{th}$, $\tau_{\text{opt}}(\tau,\gamma)\ge k_1/f_D$ is guaranteed. Since eventually we will let γ approach infinity, this assumption does not affect the design.

The average ID can then be obtained by computing

$$\begin{aligned}\tau_a(\gamma)&=\frac{2}{\pi}\int_{\beta}^{\beta+(\pi/2)}\tau_{\text{opt}}(\xi,\gamma)\,d\xi\\&=\frac{2}{\pi}\left\{\int_0^{\cos^{-1}(1/\gamma)}\frac{k_1}{f_D}\,d\theta+\int_{\cos^{-1}(1/\gamma)}^{\pi/2}\frac{k_1}{f_D}\right.\\&\quad\left.\times\left(\gamma\sin\theta+\sqrt{1-\gamma^2\cos^2\theta}\right)d\theta\right\},\quad\gamma\ge\sqrt{2}.\end{aligned}$$

There is no closed-form solution for the second term of the second integral, but it can be computed by a change of variables and approximating by a truncated Taylor expansion to get

$$\begin{aligned}\int_{\cos^{-1}(1/\gamma)}^{\pi/2}\sqrt{1-\gamma^2\cos^2\theta}\,d\theta&=\int_0^{1/\gamma}\sqrt{\gamma^2+\frac{1-\gamma^2}{1-t^2}}\,dt\\&\approx\int_0^{1/\gamma}\left(1+\frac{(1-\gamma^2)t^2}{2}\right)dt\\&=\frac{1}{\gamma}+\frac{1-\gamma^2}{6\gamma^3}.\end{aligned}$$

The average ID is then equal to

$$\tau_a(\gamma)=\frac{2k_1}{\pi f_D}\left(\cos^{-1}\frac{1}{\gamma}+1+\frac{1}{\gamma}+\frac{1-\gamma^2}{6\gamma^3}\right).\qquad(23)$$

The maximal error due to the Taylor expansion approximation can be evaluated by multiplying the integral interval and the maximum absolute value of the first omitted expansion term, which occurs when $t=1/\gamma$, to get

$$\text{Error}\le\frac{2}{\pi}\left|\frac{1}{2}(1-\gamma^2)\left(1-\frac{1}{4}(1-\gamma^2)\right)\left(\frac{1}{\gamma}\right)^4\right|\frac{1}{\gamma}.\qquad(24)$$

The maximal error occurs when $\gamma=1.378$, and the maximum error is 0.0705, which is negligible. Note that when γ approaches infinity, the maximal error approaches zero.

It can be shown that the average ID in (23) is a bounded increasing function of γ. The limit of the average ID as γ approaches infinity is

$$\tau_a=\lim_{\gamma\to\infty}\tau_a(\gamma)=\tau_{t.d.}+\frac{2k_1}{\pi f_D}=\tau_{t.d.}\left(1+\frac{2}{\pi}\right)\qquad(25)$$

which depends on f_D only. Note that only $(1+2/\pi)$ times larger ID than a single time diversity system is required for the average design. To make a comparison to the worst-case design of the previous section, we consider the same example with $f_DT=0.02$. The average ID is $\tau_a=31.3T$. For this example, we increase the ID to $43.9T$ to be at a null on the τ-axis and look at the resulting performance.

The unsafe range R_γ of γ can be computed by applying (17) to obtain $R_\gamma=[1.295,3.295]$. When the mobile is in a location whose corresponding γ parameter falls in this range, the performance is potentially degraded. The maximal percentage of possible poor performance can be computed by (19) as $q_{\max}(\tau_a)=28.697\%$. The average BEP performance is obtained the same way as the previous subsection and shown in Fig. 13. The BEP is only slightly higher than the worst case design or the ideal maximal diversity curve. However, the BEP of a four-level diversity system will not be achieved for some particular instances. The curves (a), (b), and (c) in Fig. 13 show this characteristic.

VI. Conclusion

This paper provides a space-time model for narrowband land mobile radio. The model is valid for both transmitter and receiver diversity applications. An example for receiver diversity was considered in the paper. The pairwise SEP of perfect CSI over correlated fading channels is derived, and the BPSK BEP curves are used to show the optimal AS and required ID for achieving time and receiver diversity. The important application of this work is in the area of space-time systems.

Appendix I
Cross-Correlation Function and Cross-Spectrum

In this appendix, we try to derive the space-time cross-correlation function and the cross-spectrum function of the proposed model. There are two steps to derive the cross-correlation function between two BS antennas. The first step is to express $\Delta\phi_n$ as a function of α_n and the rest of the model parameters. The second step is to take the expectation and simplify. Note that the mutual coupling effect between antennas is ignored.

Step 1: Consider the triangle $(\text{MS},P_n,\text{BS}_1)$ and $(\text{MS},P_n,\text{BS}_2)$ in Fig. 1, where P_n is the location of the nth reflector. Trigonometry dictates

$$s_1^2=a^2+d_1^2-2ad_1\cos(\pi-\beta+\alpha_n+\theta)\qquad(26)$$

$$s_2^2=a^2+d_2^2-2ad_2\cos(\pi-\beta+\alpha_n-\rho).\qquad(27)$$

Subtract (27) from (26), and with the help of the relationship in the triangle $(\text{MS},\text{BS}_1,\text{BS}_2)$ that

$$\frac{\sin(\beta+\rho)}{d_1}=\frac{\sin(\beta-\theta)}{d_2}=\frac{\sin(\theta+\rho)}{d_{sp}}\qquad(28)$$

and

$$d_{sp}=d_1\cos(\beta+\theta)-d_2\cos(\pi-\beta-\rho)\qquad(29)$$

we have

$$s_1^2-s_2^2=d_1^2-d_2^2+2ad_{sp}\cos\alpha_n.\qquad(30)$$

For typical applications in wireless communication, a far-field assumption usually holds. This means $d_1 \gg a$, $d_2 \gg a$, and $\theta \approx \rho$. Thus, from (26) and (27) we have

$$\begin{aligned} s_1 + s_2 &= d_1\sqrt{1+2\left(\frac{a}{d_1}\right)\cos(\beta-\alpha_n-\theta)+\left(\frac{a}{d_1}\right)^2} \\ &\quad + d_2\sqrt{1+2\left(\frac{a}{d_2}\right)\cos(\beta-\alpha_n+\rho)+\left(\frac{a}{d_2}\right)^2} \\ &\approx d_1 + a\cos(\beta-\alpha_n-\theta) + d_2 + a\cos(\beta-\alpha_n+\rho) \\ &\approx d_1 + d_2 + 2a\cos(\beta-\alpha_n)\cos\theta \\ &= (d_1+d_2)\left[1+\frac{2a}{d_1+d_2}\cos(\beta-\alpha_n)\cos\theta\right] \end{aligned} \tag{31}$$

and using a simple Taylor series argument, we have

$$\begin{aligned} &\frac{1}{s_1+s_2} \\ &\quad \approx \frac{1}{d_1+d_2}\left[1-\frac{2a}{d_1+d_2}\cos(\beta-\alpha_n)\cos\theta\right] \\ &\quad = \frac{1}{d_1+d_2}\left[1-\frac{2a\cos\theta}{d_1+d_2}(\cos\beta\cos\alpha_n+\sin\beta\sin\beta)\right]. \end{aligned} \tag{32}$$

Multiplying (30) by (32) and ignoring terms with $(1/(d_1+d_2))^2$ gives us

$$s_1 - s_2 \approx (d_1-d_2) + z_c\cos\alpha_n - z_s\sin\alpha_n \tag{33}$$

where

$$z_c = \frac{2a}{d_1+d_2}\left[d_{sp} - (d_1-d_2)\cos\theta\cos\beta\right] \tag{34}$$

$$z_s = \frac{2a}{d_1+d_2}(d_1-d_2)\cos\theta\sin\beta. \tag{35}$$

To gain additional intuition, the further far field assumptions of $\cos\theta \approx 1$, $(d_1+d_2) \approx 2d$ and $(d_1-d_2) \approx d_{sp}\cos\beta$ enable z_c and z_s to be approximated by

$$z_c' = \frac{a}{d}d_{sp}\sin^2\beta \tag{36}$$

$$z_s' = \frac{a}{d}d_{sp}\sin\beta\cos\beta. \tag{37}$$

$\Delta\phi_n$ can then be evaluated by $2\pi(s_1-s_2)/\lambda$.

Step 2: The cross-correlation between $c_1(t)$ and $c_2(t-\tau)$ is then

$$\begin{aligned} &R_{c_1c_2}(\tau, d_{sp}) \\ &\quad \triangleq Ec_1(t)c_2^*(t-\tau) \\ &\quad = \frac{\sigma^2}{N}E\left\{\sum_{n=1}^{N}\sum_{m=1}^{N}\exp(j2\pi f_D t[\cos(\xi-\alpha_n) \right. \\ &\qquad - \cos(\xi-\alpha_m)])\exp(j2\pi f_D\tau\cos(\xi-\alpha_m) \\ &\qquad \left. + j(\phi_n-\phi_m) + j\Delta\phi_m)\right\} \\ &\quad = \frac{\sigma^2}{N}\sum_{n=1}^{N}\exp[j2\pi f_D\tau\cos(\xi-\alpha_n)+j\Delta\phi_n] \\ &\quad = \frac{\sigma^2}{N}\sum_{n=1}^{N}\exp\left[j2\pi f_D\tau\cos(\xi-\alpha_n) \right. \\ &\qquad \left. + j\frac{2\pi}{\lambda}(d_1-d_2) + j\frac{2\pi}{\lambda}(z_c\cos\alpha_n - z_s\sin\alpha_n)\right] \\ &\quad = \frac{\sigma^2}{N}\exp\left[j\frac{2\pi}{\lambda}(d_1-d_2)\right] \\ &\qquad \times \sum_{n=1}^{N}\left\{\exp\left[j\cos\alpha_n\left(2\pi f_D\tau\cos\xi+\frac{2\pi}{\lambda}z_c\right)\right]\right. \\ &\qquad \left. \times \exp\left[j\sin\alpha_n\left(2\pi f_D\tau\sin\xi-\frac{2\pi}{\lambda}z_s\right)\right]\right\}. \end{aligned} \tag{38}$$

As the number of scatterers approaches infinity ($N \to \infty$), (38) becomes

$$\begin{aligned} \rho &= R_{c_1c_2}(\tau, d_{sp}) \\ &= \sigma^2\exp\left[j\frac{2\pi}{\lambda}(d_1-d_2)\right] \\ &\quad \times J_0\left[2\pi\sqrt{\left(f_D\tau\cos\xi+\frac{z_c}{\lambda}\right)^2+\left(f_D\tau\sin\xi-\frac{z_s}{\lambda}\right)^2}\right]. \end{aligned} \tag{39}$$

The cross-spectrum, which is defined as $S_{c_1c_2}(f, d_{sp}) \triangleq \mathcal{F}\{R_{c_1c_2}(\tau, d_{sp})\}$ where $\mathcal{F}\{\cdot\}$ is the Fourier transform with respect to τ, can be computed by first rewriting (39) as shown in (40) at the bottom of the page, and then using a result from [9, eq. (35), p. 55] to get

$$\begin{aligned} &S_{c_1c_2}(f, d_{sp}) \\ &\quad = \sigma^2\exp\left[j\frac{2\pi}{\lambda}(d_1-d_2)\right] \\ &\qquad \times \frac{\cos\left(\frac{2\pi}{\lambda f_D}(z_c\sin\xi+z_s\cos\xi)\sqrt{1-\left(\frac{f}{f_D}\right)^2}\right)}{\pi f_D\sqrt{1-\left(\frac{f}{f_D}\right)^2}}. \end{aligned} \tag{41}$$

Appendix II
Pairwise Symbol Error Probability Over Correlated Fading Channels

The space-time cross-correlation function can be applied in any design using multiple omnidirectional antennas. To demonstrate the concepts more clearly, an illustrative case of multiple

$$R_{c_1c_2}(\tau, d_{sp}) = \sigma^2 e^{j(2\pi/\lambda)(d_1-d_2)}J_0\left[2\pi f_D\sqrt{\left(\tau+\frac{z_c\cos\xi}{\lambda f_D}-\frac{z_s\sin\xi}{\lambda f_D}\right)^2+\left(\frac{z_c\sin\xi}{\lambda f_D}+\frac{z_s\cos\xi}{\lambda f_D}\right)^2}\right] \tag{40}$$

TABLE I
PAIRWISE SEP OVER TWO CORRELATED FADING CHANNELS

$0 < \|\rho\| < 1$ (correlated fading)	$\|\rho\| = 0$ (independent fading)
$\mathrm{P}_{d_i}\{d_i \to d_j\} = \frac{\lambda_2^3}{(\lambda_2-\lambda_4)(\lambda_2-\lambda_1)(\lambda_2-\lambda_3)} + \frac{\lambda_4^3}{(\lambda_4-\lambda_1)(\lambda_4-\lambda_2)(\lambda_4-\lambda_3)}$	$\mathrm{P}_{d_i}\{d_i \to d_j\} = \frac{\lambda_2^2(3\lambda_1-\lambda_2)}{(\lambda_1-\lambda_2)^3}$
$\lambda_1 = z_1 + \sqrt{z_1^2+z_2} > 0, \quad \lambda_2 = z_1 - \sqrt{z_1^2+z_2} < 0$ $\lambda_3 = z_3 + \sqrt{z_3^2+z_4} > 0, \quad \lambda_4 = z_3 - \sqrt{z_3^2+z_4} < 0$ $z_1 = \sigma^2 E_s(1+\|\rho\|)\left(\mathcal{R}e\left\{\|d_i\|^2 - d_i d_j^*\right\} - \frac{\|d_i\|^2-\|d_j\|^2}{2}\right)$ $z_2 = \sigma^2 E_s(1+\|\rho\|)N_0\|d_i-d_j\|^2$ $z_3 = \sigma^2 E_s(1-\|\rho\|)\left(\mathcal{R}e\left\{\|d_i\|^2 - d_i d_j^*\right\} - \frac{\|d_i\|^2-\|d_j\|^2}{2}\right)$ $z_4 = \sigma^2 E_s(1-\|\rho\|)N_0\|d_i-d_j\|^2$	$\lambda_1 = z_1 + \sqrt{z_1^2+z_2} > 0$ $\lambda_2 = z_1 - \sqrt{z_1^2+z_2} < 0$ $z_1 = \sigma^2 E_s\left(\mathcal{R}e\left\{\|d_i\|^2 - d_i d_j^*\right\} - \frac{\|d_i\|^2-\|d_j\|^2}{2}\right)$ $z_2 = \sigma^2 E_s N_0\|d_i-d_j\|^2$

TABLE II
BEP OF BPSK SIGNAL OVER TWO CORRELATED FADING CHANNELS. G_b DENOTES E_b/N_0

$0 < \|\rho\| < 1$ (correlated fading)	$\|\rho\| = 0$ (independent fading)
$\mathrm{BEP} = \frac{\lambda_2^3}{(\lambda_2-\lambda_4)(\lambda_2-\lambda_1)(\lambda_2-\lambda_3)} + \frac{\lambda_4^3}{(\lambda_4-\lambda_1)(\lambda_4-\lambda_2)(\lambda_4-\lambda_3)}$	$\mathrm{BEP} = \frac{\lambda_2^2(3\lambda_1-\lambda_2)}{(\lambda_1-\lambda_2)^3}$
$\lambda_1 = (1+\|\rho\|)\left(1+\sqrt{1+\frac{1}{\sigma^2 G_b(1+\|\rho\|)}}\right) > 0$ $\lambda_2 = (1+\|\rho\|)\left(1-\sqrt{1+\frac{1}{\sigma^2 G_b(1+\|\rho\|)}}\right) < 0$ $\lambda_3 = (1-\|\rho\|)\left(1+\sqrt{1+\frac{1}{\sigma^2 G_b(1-\|\rho\|)}}\right) > 0$ $\lambda_4 = (1-\|\rho\|)\left(1-\sqrt{1+\frac{1}{\sigma^2 G_b(1-\|\rho\|)}}\right) < 0$	$\lambda_1 = 1+\sqrt{1+\frac{1}{\sigma^2 G_b}} > 0$ $\lambda_2 = 1-\sqrt{1+\frac{1}{\sigma^2 G_b}} < 0$

receiving antennas with perfect CSI is analyzed in detail. The channel model equation for such a system can be represented as

$$\underline{r}(n) = \sqrt{E_s}\underline{c}(n)d(n) + \underline{n}(n) \tag{42}$$

where $\underline{r}(n) = [r_1(n), r_2(n), \cdots, r_L(n)]^T$ is the received nth symbols at each antenna, L denotes the number or receiving antennas, and $E_s = mE_b/E_{avg}$ is the transmitted symbol energy where m is the number of bits per symbol, E_b is the energy per bit, and E_{avg} is the constellation average energy. $\underline{c}(n) = [c_1(n), c_2(n), \cdots, c_L(n)]^T$ is the corresponding multiplicative distortion, $d(n)$ is the transmitted symbol and is chosen from an alphabet set $\boldsymbol{D}$, and $\underline{n}(n) = [n_1(n), n_2(n), \cdots, n_L(n)]^T$ is the additive white Gaussian noise, where $n_1(n)$ through $n_L(n)$ are all independent. For notational simplicity, the argument n will be dropped in the following derivation.

The model is equivalent to transmitting a rate $1/L$ repetition code over single antenna channel, but without increasing the transmitting power L times for each information symbol. The optimal maximum likelihood decision can be easily shown as

$$\begin{aligned}\hat{d} &= \arg\max_{d\in\boldsymbol{D}}\{\ln[f(\underline{r}\,|\,\underline{c}, d)]\} \\ &= \arg\max_{d\in\boldsymbol{D}}\left\{-\left(\underline{r} - \sqrt{E_s}\underline{c}d\right)^H\left(\underline{r} - \sqrt{E_s}\underline{c}d\right)\right\} \\ &= \arg\max_{d\in\boldsymbol{D}}\left\{2\sqrt{E_s}\cdot\mathrm{Re}\{\underline{r}^H\underline{c}d\} - E_s|d|^2\underline{c}^H\underline{c}\right\}\end{aligned} \tag{43, 44}$$

where $\arg\max\{\cdot\}$ denotes the value of the argument that maximizes the function, $f(\cdot)$ is the probability density function, the superscript H denotes transposed complex conjugate, and $\mathrm{Re}\{\cdot\}$ denotes the real part of a complex value.

In computing the pairwise SEP, it is not correct to assume that c_1 through c_L are uncorrelated. The pairwise SEP for the receiver diversity system in correlated fading can be computed by applying the algorithm in [10] and [11]. Let $P_{d_i}\{d_i \to d_j\}$ denote the pairwise error probability of decoding d_j over d_i given d_i was transmitted, then

$$\begin{aligned}P_{d_i}\{d_i \to d_j\} &= P_{d_i}\left\{2\sqrt{E_s}\cdot\mathrm{Re}\{\underline{r}^H\underline{c}d_j\} - E_s|d_j|^2\underline{c}^H\underline{c}\right. \\ &\qquad \left. > 2\sqrt{E_s}\cdot\mathrm{Re}\{\underline{r}^H\underline{c}d_i\} - E_s|d_i|^2\underline{c}^H\underline{c}\right\} \\ &= P_{d_i}\left\{\underline{z}_{d_i}^H\boldsymbol{Q}_{d_i,d_j}\underline{z}_{d_i} < 0\right\}\end{aligned} \tag{45}$$

where $\underline{z}_{d_i} = [\underline{r}^T, \underline{c}^T]^T$ (given d_i was transmitted),

$$\boldsymbol{Q}_{d_i,d_j} = \begin{bmatrix} \mathbf{0}_L & \sqrt{E_s}(d_i-d_j)\cdot\boldsymbol{I}_L \\ \sqrt{E_s}(d_i-d_j)^*\cdot\boldsymbol{I}_L & -E_s(|d_i|^2-|d_j|^2)\cdot\boldsymbol{I}_L \end{bmatrix}$$

$\mathbf{0}_L$ is an $L\times L$ zero matrix, $\boldsymbol{I}_L$ is an $L\times L$ identity matrix, and L denotes the number of receiving antennas.

Let $g = \underline{z}_{d_i}^H Q_{d_i,d_j} \underline{z}_{d_i}$, and $f(g)$ be the density function of g, then $f(g)$ can be represented as the inverse Laplace transformation of its moment generating function, i.e.,

$$f(g) = \frac{1}{2\pi j} \oint_C \phi(s) \exp(sg)\, ds \tag{46}$$

where

$$\begin{aligned} \phi(s) &= E\left\{\exp\left(-s\underline{z}_{d_i}^H \boldsymbol{Q}_{d_i,d_j}\underline{z}_{d_i}\right)\right\} \\ &= \frac{1}{\det\left[\boldsymbol{I}_{2L} + s\boldsymbol{C}_{\underline{z}_{d_i}}\boldsymbol{Q}_{d_i,d_j}\right]} \end{aligned} \tag{47}$$

$\boldsymbol{I}_{2L}$ is a $2L \times 2L$ identity matrix and $\boldsymbol{C}_{\underline{z}_{d_i}} = E\underline{z}_{d_i}\underline{z}_{d_i}^H$.

Substituting (47) in (46), and applying the residue theorem, gives

$$\begin{aligned} P_{d_i}\{d_i \to d_j\} &= \int_{-\infty}^{0} f(g)\, dg \\ &= \frac{1}{2\pi j}\int_{s=\omega-j\infty}^{\omega+j\infty} \frac{\phi(s)}{s}\, ds \\ &= -\sum \text{Residue}\left[\frac{\phi(s)}{s}\right]_{\text{Right Plane Poles}} \end{aligned} \tag{48}$$

where ω is some constant satisfying $0 < \omega <$ [the real part of the first right plane pole of $\phi(s)$].

A closed-form pairwise SEP can be further derived [8]. The result of the pairwise SEP over two correlated fading channels is listed in Table I. Note that the pairwise SEP for independent fading is the same as what is derived in [12]. A closed-form BEP for BPSK signal can be obtained by substituting in $d_i = 1$ and $d_j = -1$ in Table II, and noting $E_s = E_b$. The result is listed in Table II where $G_b \triangleq E_b/N_0$. The BPSK signal will be used for discussions throughout this paper for its simplicity. The generalization of these discussions to denser constellations is straightforward and is detailed in [8].

REFERENCES

[1] J.-C. Guey, M. P. Fitz, M. R. Bell, and W.-Y. Kuo, "Signal design for transmitter diversity wireless communication systems over Rayleigh fading channel," *IEEE Trans. Commun.*, vol. 47, pp. 527–537, Apr. 1999.

[2] V. Tarokh, N. Seshadri, and A. Calderbank, "Space-time codes for high data rate wireless communication: Performance criterion and code construction," *IEEE Trans. Inform. Theory*, vol. 44, pp. 744–765, Mar. 1998.

[3] W. Jakes, *Microwave Mobile Communications*. New York: Wiley, 1974.

[4] R. H. Clarke, "A statistical theory of mobile-radio reception," *Bell Syst. Tech. J.*, pp. 957–1000, July–Aug. 1968.

[5] T. Aulin, "A modified model for the fading signal at a mobile radio channel," *IEEE Trans. Veh. Technol.*, vol. 28, pp. 182–203, 1979.

[6] A. Turkmani and J. D. Parsons, "Characterization of mobile radio signals: Model description," *IEEE Proc.-I*, vol. 138, pp. 549–556, Dec. 1991.

[7] ——, "Characterization of mobile radio signals: Base station crosscorrelation," *IEEE Proc.-I*, vol. 138, pp. 557–565, Dec. 1991.

[8] T.-A. Chen, "Space-time characteristics of frequency nonselective Rayleigh fading channels with applications to modeling, system design, and demodulation," Ph.D. dissertation, School Elec. Computer Eng., Purdue Univ., 1998.

[9] H. Bateman, *Tables of Integral Transforms*. New York: McGraw-Hill, 1954.

[10] J. Pierce and S. Stein, "Multiple diversity with nonindependent fading," in *Proc. IRE*, 1960, pp. 89–104.

[11] W.-Y. Kuo and M. P. Fitz, "Design and analysis of transmitter diversity using intentional frequency offset for wireless communications," *IEEE Trans. Veh. Tech.*, vol. 46, pp. 871–881, Nov. 1997.

[12] J. G. Proakis, *Digital Communications*. New York: McGraw-Hill, 1995.

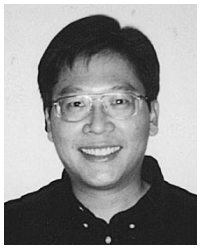

Tai-Ann Chen (S'96–M'98) received the B.S.E.E. and B.S.I.E. double-major degrees with the highest honor from National Tsing Hua University, Taiwan, in 1989, and the M.S.E.E. and Ph.D. degrees from the School of Electrical and Computer Engineering, Purdue University, West Lafayette, IN, in 1994 and 1998, respectively. He joined the Wireless System Core Technology Department, Lucent Technologies, Whippany, NJ, as a Member of the Technical Staff in 1998, and is currently working on the 3G CDMA2000 system algorithms design and analysis.

Dr. Chen was heavily involved in the design and implementation of a prototype wireless modem during his graduate study. He also participated in a summer project of the CDMA system analysis at Lucent Technologies in 1997. His research interests include the mobile wireless communications theory and its applications on both wideband and narrowband systems. His current focuses are on the fading channel characteristic and channel estimation, CDMA system power control algorithm analysis, and the space-time coding technique. Dr. Chen has one U.S. patent submission under the examination of the U.S. patent office.

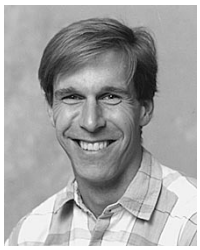

Michael P. Fitz (S'86–M'89) received the B.E.E. degree (*summa cum laude*) from the University of Dayton, Dayton, OH, in 1983, and the M.S. and Ph.D. degrees in electrical engineering from the University of Southern California in 1984 and 1989, respectively.

He was employed at Hughes Aircraft Co., Fullerton, CA and TRW Inc., Redondo Beach, CA while in graduate school. In 1989, he accepted an Assistant Professorship with the School of Electrical Engineering at Purdue University, was promoted to an Associate Professor in 1995. He accepted a position as an Associate Professor at the Ohio State University (OSU) in Columbus, OH and began full time at OSU in 1997. His research is in the broad area of statistical communication theory. A major component of his research program is physical layer communications theory for mobile wireless communications. This effort focuses on modulation, coding, demodulation, synchronization, and equalization techniques optimized for mobile or vehicular digital communications. His current interests include space-time coding theory, channel estimation, synchronization and demodulation and decoding algorithms for narrowband and time division multiplexed wireless data transmission.

Dr. Fitz is Member of the Information Processing Systems (IPS) Laboratory at OSU and has directed the formation of the Wireless Communications Laboratory within IPS. The laboratory develops algorithms for, analyzes performance, and develops breadboard testbeds of wireless communication radio modems and networks.

Wen-Yi Kuo (S'92–M'95–SM'00) received the Ph.D. degree in electrical engineering from Purdue University, West Lafayette, IN; in 1994, the M.S.E.E. from National Taiwan University, and the B.S. degree from National Chiao Tung University, Taiwan.

From January 1995 to April 1999, he was with Radio Performance and Optimization Dept and then Wireless Systems Core Technologies Department of Lucent Technologies working on 2G and 3G CDMA performance analysis, algorithms, system engineering, and deployment study. Projects include soft handoff, inter-frequency handoff, power control, rake receiver, radio resource control, access and paging, distributed antenna systems, mobile location estimation, and capacity/coverage analysis. During April 1999 to May 2000 he was with Wireless Communications Research Department of AT&T Labs and worked on WCDMA related research. Since June 2000, he has been with Wiscom Technologies, Clark, NJ, working on high-speed data wireless modem. His research interests include fading channel modeling, physical layer communication, radio resource control, and system deployment optimization.

He holds three U.S. patents and has another 32 patent submissions under examination in the U.S. patent and trademark office. He was an adjunct professor on New Jersey Institute of Technologies in 1998 and taught the graduate course Personal Communications Systems. He codeveloped a series of three day courses on 3G wireless technologies for Lucent internal education in 1998.

Dr. Kuo is and editor for IEEE JOURNAL ON SELECTED AREAS IN COMMUNICATIONS (JSAC) wireless series, was a board member of Chinese Institute of Engineers—USA, New York chapter in 1999, and is a member of Telecommunication Advisory Board, Ministry of Traffic and Communications, Taiwan.

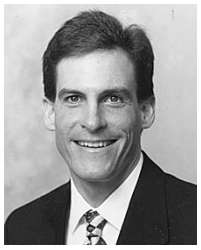

Michael D. Zoltowski (S'79–M'86–SM'95–F'99) was born in Philadelphia, PA, on August 12, 1960. He received both the B.S. and M.S. degrees in electrical engineering (with highest honors) from Drexel University in 1983 and the Ph.D. degree in systems engineering from the University of Pennsylvania in 1986.

In Fall 1986, he joined the faculty of Purdue University where he currently holds the position of Professor of Electrical and Computer Engineering.

Dr. Zoltowski was the recipient of the IEEE Signal Processing Society's 1991 Paper Award (Statistical Signal and Array Processing Area) and "The Fred Ellersick MILCOM Award for Best Paper in the Unclassified Technical Program" at the IEEE Military Communications (MILCOM'98) Conference. He is a contributing author to *Adaptive Radar Detection and Estimation*, Wiley, 1991, *Advances in Spectrum Analysis and Array Processing, Vol. III*, Prentice-Hall, 1994, and *CRC Handbook on Digital Signal Processing*, CRC Press, 1996. He has served as an Associate Editor for both the IEEE TRANSACTIONS ON SIGNAL PROCESSING and the *IEEE Communications Letters*. Within the IEEE Signal Processing Society, he has been a Member of the Technical Committee for the Statistical Signal and Array Processing Area, and is currently a Member of both the Technical Committee for Communications and the Technical Committee on DSP Education. In addition, he is currently a Member-at-Large of the Board of Governors and Secretary of the IEEE Signal Processing Society. His present research interests include space-time adaptive processing for all areas of mobile and wireless communications, GPS, and radar.

Jimm H. Grimm was born in New Jersey in 1968. He received the B.S.E.E. degree from Rose-Hulman Institute of Technology in 1990, the M.S.E.E. degree from the Illinois Institute of Technology in 1992, and the Ph.D. degree from Purdue University in 1998.

While at Purdue he was a key figure in the design, analysis, implementation, and field testing of a prototype wireless mobile modem. In 1989 and 1990, he held an internship at Ford Motor Company troubleshooting and documenting PLC programs on assembly line robotics. Currently he is employed at Grayson Wireless, where he is working on maximum likelihood location estimation for wireless 911 calls. His research interests in fading channel communications include estimation theory, synchronization, and error control coding.